

## Exclusive photoproduction of large momentum-transfer $K$ and $K^*$ mesons

P. Kroll\* and M. Schürmann†

*Fachbereich Physik, Universität Wuppertal, D-42097 Wuppertal, Germany*

K. Passek‡

*Rudjer Bošković Institute, P.O. Box 1016, HR-10000 Zagreb, Croatia*

W. Schweiger§

*Institut für Theoretische Physik, Universität Graz, A-8010 Graz, Austria*

(Received 16 April 1996)

The reactions  $\gamma p \rightarrow K^+ \Lambda$  and  $\gamma p \rightarrow K^{*+} \Lambda$  are analyzed within perturbative QCD, allowing for diquarks as quasidelementary constituents of baryons. The diquark-model parameters and the quark-diquark distribution amplitudes of the proton and  $\Lambda$  are taken from previous investigations of electromagnetic baryon form factors and Compton scattering off protons. Unpolarized differential cross sections and polarization observables are computed for different choices of the  $K$  and  $K^*$  distribution amplitudes. The asymptotic form of the  $K$  distribution amplitude ( $\propto x_1 x_2$ ) is found to provide a satisfactory description of the  $K$  photoproduction data. [S0556-2821(97)00307-X]

PACS number(s): 13.60.Le, 12.38.Bx

### I. INTRODUCTION

The reactions  $\gamma p \rightarrow KY$  ( $Y = \Lambda, \Sigma$ ) belong to the most elementary processes which allow one to study strangeness production. Stimulated by the advent of a new generation of intermediate-energy electron facilities, such as the Bonn accelerator ELSA or the Continuous Electron Beam Accelerator Facility (CEBAF), they recently received renewed interest. Traditional hadronic models applied to the analysis of  $K$  photoproduction mostly make use of Feynman-diagram techniques [1–3]. The corresponding reaction mechanism is based on the exchange of  $p$ ,  $\Lambda$ ,  $\Sigma$ ,  $K$ , and  $K^*$ , along with a varying number of  $N^*$  and  $Y^*$  resonances. Apart from some problems with SU(3) bounds on the hadronic coupling constants  $g_{KYN}$  [4], such models seem to work properly for photon energies up to  $p_{\text{lab}}^\gamma \lesssim 1.4\text{--}2.2$  GeV. New data of higher precision and completeness (which include also spin observables) [5,6] are expected to restrict still persisting uncertainties in the meson-baryon couplings and the resonance parameters.

A more fundamental treatment of photoproduction should, of course, rely on QCD, the dynamics of interacting quarks and gluons. A step in this direction are effective, ‘‘QCD-inspired’’ models which include already one or the other feature of QCD. A particular example is the chiral quark model which has been applied to  $K$  photoproduction very recently [7]. Its elementary degrees of freedom are constituent quarks and the members of the (lowest-lying) pseudoscalar meson octet ( $K$ ,  $\eta$ , and  $\pi$ ). The latter are considered Goldstone bosons associated with the spontaneous breaking of chiral symmetry. The (confined) quarks interact

via exchange of the Goldstone bosons. With less parameters than hadronic approaches this model also provides reasonable results for  $p_{\text{lab}}^\gamma \lesssim 2$  GeV. Its restricted range of validity is caused by the use of nonrelativistic transition operators and baryon wave functions.

Direct application of QCD is (until now) restricted to kinematical situations in which the scattering of the hadronic constituents and their hadronization takes place on rather different scales. In general this means large energies and momentum transfers ( $p_\perp$ ). Well beyond the resonance region ( $p_{\text{lab}}^\gamma \gg 1$  GeV) exclusive photoproduction cross sections exhibit a characteristic angular dependence. At forward (small  $t$ ) and backward (small  $u$ ) angles the strong variation of the differential cross section is adequately reproduced by the exchange of meson and baryon Regge trajectories, respectively [8]. Around  $\theta_{\text{c.m.}} = 90^\circ$  (large  $t$  and  $u$ ) the cross section flattens and shows (for fixed angles) an energy dependence typical for a hard interaction between the photon and the constituents inside the proton. A constituent scattering model for high-energy, large- $p_\perp$  elastic and quasielastic reactions has been proposed in Ref. [9]. The interaction mechanism of this model, namely quark interchange, may be also thought of as one of the simplest ways to describe photoproduction of open strangeness. The resulting interchange amplitude is just a convolution over light-cone wave functions of the interacting quarks, which have to be parametrized in an appropriate way.

A more subtle picture, often called the ‘‘hard-scattering approach,’’ emerges if one tries to figure out the leading twist contributions to hard exclusive processes within perturbative QCD [10]. The outcome of such an analysis is a factorization formula which is also expressed as a convolution integral. This integral now consists of distribution amplitudes (DA’s) and a hard-scattering amplitude. The process-dependent hard-scattering amplitude is perturbatively calculable and represents the scattering of the hadronic constituents in collinear approximation. The process-

\*Electronic address: kroll@wpts0.physik.uni-wuppertal.de

†Present address: Deutsche Bank, Frankfurt.

‡Electronic address: passek@thphys.irb.hr

§Electronic address: schweigerw@edvz.kfunicg.ac.at

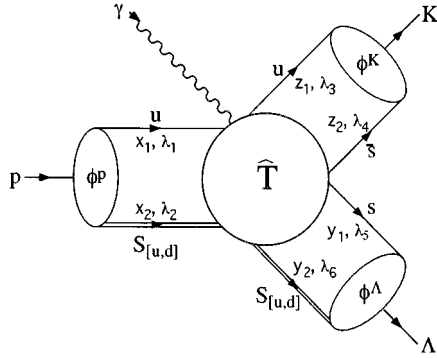


FIG. 1. Constituent kinematics for  $\gamma p \rightarrow K^{(*)} \Lambda$ .

independent DA's contain the nonperturbative bound-state dynamics of the hadronic constituents. DA's are, roughly speaking, valence Fock-state wave functions integrated over the transverse momentum. At present, the knowledge on hadron DA's is still rather limited. The main information is provided by QCD sum-rule techniques which give estimates of the lowest moments of various meson and baryon DA's [11–13]. The few lowest moments impose some restrictions on the shape of the DA's but do not determine them uniquely. A thorough discussion on how to construct model DA's reproducing a certain number of moments can be found in Ref. [14]. One should also note that the DA's constrained by QCD sum rules are subject to severe criticism [15–18]. Thus, one is forced, at present, to supplement the lack of theoretical knowledge on DA's by some input coming from experiment. Photoproduction reactions are, in this respect, certainly very interesting. They exhibit a rich flavor structure and are still simple enough to allow for the computation of all the Feynman diagrams which enter the hard-scattering amplitude. Perturbative QCD predictions for various photoproduction channels have been published in Ref. [19]. This paper discusses also the sensitivity of the results on the choice of the hadron DA's. Apart from the fact that there are objections to the numerics of this work (cf. Sec. IV) and it still needs confirmation, the predictions for the  $K\text{-}\Lambda$  channel occur to be in considerable disagreement with experiment.

The present work concentrates on photoproduction of the  $K\text{-}\Lambda$  and  $K^*\text{-}\Lambda$  final states. We consider these reactions within a particular version of the hard-scattering approach in which baryons are treated as quark-diquark systems. The same approach has already been applied successfully to other photon-induced hadronic reactions like magnetic and electric baryon form factors in the space- [20] and timelike region [21], real and virtual Compton scattering [22], and two-photon annihilation into proton-antiproton [21]. Further applications of the diquark model include the charmonium decay  $\eta_c \rightarrow p\bar{p}$  [21] and the calculation of Landshoff contributions in elastic proton-proton scattering [23]. The introduction of diquarks not only simplifies computations, but is rather motivated by the requirement to extend the hard-scattering approach from large down to intermediate momentum transfers ( $p_\perp^2 \gtrsim 4 \text{ GeV}^2$ ). This is the momentum-transfer region where experimental data are still available, but where still persisting nonperturbative effects prevent the pure quark hard-scattering approach to become fully operational. Di-

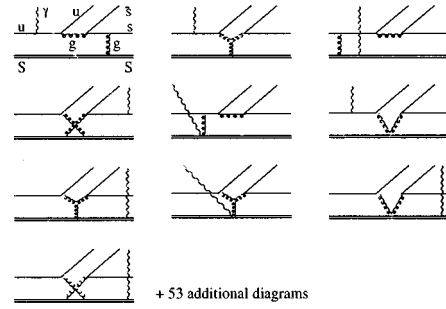


FIG. 2. A few representative examples of Feynman diagrams contributing to the elementary process  $\gamma u S_{[u,d]} \rightarrow u \bar{s} s S_{[u,d]}$ .

quarks may be considered as an effective way to cope with such nonperturbative effects. It is an assumption that, on an intermediate momentum-transfer scale, two of the three valence quarks in a baryon make up a diquark cluster. However, from many experimental and theoretical approaches there have been indications suggesting the presence of diquarks. For instance, they were introduced in baryon spectroscopy, in nuclear physics, in jet fragmentation, and in weak interactions to explain the famous  $\Delta I = 1/2$  rule. Diquarks also provide a natural explanation of the equal slopes of meson and baryon Regge trajectories. For more details and for references, see [24]. It is important to note that QCD provides some attraction between two quarks in a color  $\{\bar{3}\}$  state at short distances as is to be seen from the static reduction of the one-gluon exchange term. Also the instanton force seems to lead to diquark formation [25]. Even more important for our aim, diquarks have also been found to play a role in inclusive hard-scattering reactions. The most obvious place to signal their presence is deep-inelastic lepton-nucleon scattering. Indeed the higher twist terms, convincingly observed [26], can be modeled as lepton-diquark elastic scattering. Baryon production in inclusive  $p\text{-}p$  collisions also clearly reveals the need for diquarks scattered elastically in the hard elementary reactions [27]. For instance, kinematical dependencies or the excess of the proton yield over the antiproton yield find simple explanations in the diquark model. No other explanation of these phenomena is known as yet.

The main ingredients of the diquark model are baryon DA's in terms of quarks and diquarks, the coupling of gluons and photons to diquarks, and, in order to account for the composite nature of diquarks, phenomenological diquark form factors. The proper choice of the diquark form factors guarantees the compatibility of the diquark model with the pure quark hard-scattering approach in the limit  $p_\perp \rightarrow \infty$ . In so far as the pure quark picture of Brodsky-Lepage and the diquark model do not oppose each other, they are not alternatives but rather complements. The model parameters have been determined in Ref. [20] by means of elastic electron-nucleon scattering data. The full model incorporates scalar ( $S$ ) and vector diquarks. Vector diquarks are important for the description of spin observables which violate hadronic helicity conservation, i.e., quantities not explicable within the pure quark hard-scattering approach. The nice and simplifying feature of the two photoproduction reactions we are interested in is that they are not influenced by vector di-

quarks since only the  $S_{[u,d]}$  diquark is common to proton and  $\Lambda$ .

The following section starts with an outline of the hard-scattering approach with (scalar) diquarks. It contains also a description of the kaon, proton, and  $\Lambda$  DA's to be used in the sequel. Section III deals with the constituent kinematics, photoproduction observables, and the general structure of photoproduction helicity amplitudes within the diquark model. Predictions for photoproduction observables with a discussion of their dependence on the choice of the kaon DA

can be found in Sec. IV. Conclusions and prospects are given in Sec. V. Analytical expressions for the helicity amplitudes are tabulated in Appendix A. Our numerical method for treating propagator singularities is sketched in Appendix B.

## II. HARD SCATTERING WITH DIQUARKS

Within the hard-scattering approach a helicity amplitude  $M_{\{\lambda\}}$  for the reaction  $\gamma p \rightarrow K^{(*)+} \Lambda$  is (to leading order in  $1/p_\perp$ ) given by the the convolution integral [10]

$$M_{\{\lambda\}}(\hat{s}, \hat{t}) = \int_0^1 dx_1 dy_1 dz_1 \phi^{K^{(*)+}}(z_1, \tilde{Q}) \phi^{\Lambda^+}(y_1, \tilde{Q}) \hat{T}_{\{\lambda\}}(x_1, y_1, z_1; \hat{s}, \hat{t}) \phi^p(x_1, \tilde{Q}). \quad (2.1)$$

The distribution amplitudes  $\phi^H$  are probability amplitudes for finding the valence Fock state in the hadron  $H$  with the constituents carrying certain fractions of the momentum of their parent hadron and being collinear up to a factorization scale  $\tilde{Q}$ . In our model the valence Fock state of an ordinary baryon is assumed to consist of a quark and a diquark ( $D$ ). We fix our notation in such a way that the momentum fraction appearing in the argument of  $\phi_H$  is carried by the quark—with the momentum fraction of the other constituent (either diquark or antiquark) it sums up to 1 (cf. Fig. 1). In what follows we will neglect the (logarithmic)  $\tilde{Q}$  dependence of the DA's since it is of minor importance in the restricted energy range we will be interested in. The hard-scattering amplitude  $\hat{T}_{\{\lambda\}}$  is calculated perturbatively in collinear approximation and consists in our particular case of all possible tree diagrams contributing to the elementary scattering process  $\gamma u S \rightarrow u \bar{s} s S$ . A few examples of such diagrams are depicted in Fig. 2. The subscript  $\{\lambda\}$  represents the set of possible photon, proton, and  $\Lambda$  helicities. We have written the Mandelstam variables  $s$  and  $t$  with a hat to indicate that masses are neglected during the calculation of the hard-scattering amplitude. They are only taken into account in flux and phase-space factors.

If one assumes zero relative orbital angular momentum between quark and diquark and takes advantage of the collinear approximation [ $p_q = x_1 p_B$  and  $p_D = x_2 p_B = (1-x_1)p_B$ ] the valence Fock-state wave function of a baryon  $B$  belonging to the energetically lowest-lying octet may be written as

$$\begin{aligned} \Psi^B(p_B; \lambda) &= f_S^B \phi_S^B(x_1) \chi_S^B u(p_B, \lambda) \\ &+ f_V^B \phi_V^B(x_1) \chi_V^B \frac{1}{\sqrt{3}} \left( \gamma^\alpha + \frac{p_B^\alpha}{m_B} \right) \gamma_5 u(p_B, \lambda). \end{aligned} \quad (2.2)$$

The two terms in Eq. (2.2) represent configurations consisting of a quark and either a scalar or vector diquark. The pleasant feature of the covariant wave-function representation Eq. (2.2) is that it contains, in addition to  $x_1$  and  $\alpha$  (the

Lorentz index of the vector-diquark polarization vector), only baryonic quantities (momentum  $p_B$ , helicity  $\lambda$ , baryon mass  $m_B$ ).

For an SU(6)-like spin-flavor dependence the flavor functions  $\chi$  for proton and  $\Lambda$  take on the form (the notation should be obvious)

$$\chi_V^p = u S_{[u,d]}, \quad \chi_V^p = [u V_{\{u,d\}} - \sqrt{2} d V_{\{u,u\}}] / \sqrt{3}, \quad (2.3)$$

$$\chi_S^\Lambda = [u S_{[d,s]} - d S_{[u,s]} - 2s S_{[u,d]}] / \sqrt{6},$$

$$\chi_V^\Lambda = [u V_{\{d,s\}} - d V_{\{u,s\}}] / \sqrt{2}. \quad (2.4)$$

Similarly, also the  $q\bar{q}$  wave functions of pseudoscalar (PM) and vector (VM) mesons may be represented in a covariant way:

$$\Psi^{PM}(p_{PM}) = f^{PM} \phi^{PM}(x_1) \chi^{PM} \frac{1}{\sqrt{2}} (\not{p}_{PM} + m_{PM}) \gamma_5, \quad (2.5)$$

$$\begin{aligned} \Psi^{VM}(p_{VM}; \lambda) &= -f^{VM} \phi^{VM}(x_1, \lambda) \chi^{VM} \\ &\times \frac{1}{\sqrt{2}} (\not{p}_{VM} + m_{VM}) \not{\epsilon}(\lambda), \end{aligned} \quad (2.6)$$

with the flavor function of the  $K^{(*)+}$  meson given by

$$\chi^{K^{(*)+}} = u \bar{s}. \quad (2.7)$$

At this point we are already in the position to recognize a considerable simplification in the treatment of the reaction  $\gamma p \rightarrow K^{(*)+} \Lambda$  as compared to arbitrary photoproduction processes. Photoproduction of the  $K^{(*)+} \Lambda$  final state can solely proceed via the  $S_{[u,d]}$  diquark. This is the only kind of diquark occurring in both the proton and the  $\Lambda$  wave function [cf. Eqs. (2.3) and (2.4)]. The opposite situation, namely that only the  $V_{\{u,d\}}$  diquark becomes involved, holds for  $\gamma p \rightarrow K^{(*)+} \Sigma^0$ . The fact that scalar diquarks as well as (massless) quarks do not change their helicity when interacting with a gluon imposes already strong restrictions on spin observables of the  $K^+ \Lambda$  and  $K^{*+} \Lambda$  channels. Helicity

amplitudes which require the flip of the baryonic helicity are predicted to vanish, e.g., for the  $\gamma p \rightarrow K^+ \Lambda$  process. On the other hand, helicity flips may take place in the  $\gamma p \rightarrow K^+ \Sigma^0$  reaction by means of the vector diquark. In order to work out the different features of scalar and vector diquarks a comparison of the  $\Lambda$  and  $\Sigma^0$  photoproduction channels would certainly be of great benefit.

The complicated, nonperturbative bound-state dynamics is contained in the DA's  $\phi^H$ . These are light-cone wave functions integrated over transverse momentum (up to  $\tilde{Q}$ ). The  $r=0$  values of the corresponding configuration space wave functions are related to the constants  $f^H$ . We will check the sensitivity of our photoproduction calculation on the shape of the  $K$  ( $K^*$ ) DA by choosing two qualitatively rather different forms: the one is the asymptotic DA,

$$\phi_{\text{asy}}(x) = 6x(1-x) \quad , \quad (2.8)$$

which solves the  $\tilde{Q}$  evolution equation for  $\phi(x, \tilde{Q})$  in the limit  $\tilde{Q} \rightarrow \infty$  (see, e.g., Ref. [10]); the other one is a two-humped DA, namely

$$\phi_{\text{CZ}}^K(x) = N^K \phi_{\text{asy}}(x) [0.08 + 0.6(1-2x)^2 + 0.25(1-2x)^3] \quad , \quad (2.9)$$

for the  $K$ ,

$$\phi_L^{K^*}(x) = N_L^{K^*} \phi_{\text{asy}}(x) [0.18 + 0.1(1-2x)^2 + 0.41(1-2x)^3] \quad , \quad (2.10)$$

for the longitudinally polarized  $K^*$ , and

$$\phi_T^{K^*}(x) = N_T^{K^*} \phi_{\text{asy}}(x) [0.284 + 0.07(1-2x) - 0.534(1-2x)^2 + 0.21(1-2x)^3 + 0.267(1-2x)^4] \quad , \quad (2.11)$$

for the transversally polarized  $K^*$ . The DA's, Eqs. (2.9)–(2.11), have been proposed in Refs. [11,28]. They reproduce the corresponding QCD sum-rule moments at  $\tilde{Q}^2 = 0.25 \text{ GeV}^2$ . It has been demonstrated quite recently that the linear  $x$  dependence of pseudoscalar meson DA's at the end points  $x \rightarrow 0, 1$  can be considered as a direct consequence of QCD [29].

The usual normalization condition,  $\int_0^1 dx \phi^H(x) = 1$ , fixes the constants  $N$  in Eqs. (2.9)–(2.11). The quantities  $f^{PM}$  and  $f^{VM}$  showing up in Eqs. (2.5) and (2.6) are related to experimentally determinable decay constants of the corresponding mesons. From the  $K^+ \rightarrow \mu^+ \nu_\mu$  decay one infers in particular that  $f^{K^+} = f_{\text{decay}}^{K^+} / 2\sqrt{6} = 32.6 \text{ MeV}$ . The value of  $f^{K^*}$  is only known indirectly via the QCD sum-rule result  $f^{K^*} = 1.05 f^p$  (cf. Ref. [11]). The experimental value of  $f^p = f_{\text{decay}}^p / 2\sqrt{6} = 40.8 \text{ MeV}$  obtained from the  $\rho^0 \rightarrow e^+ e^-$  decay implies  $f^{K^*} = 42.9 \text{ MeV}$ .

In previous applications of the diquark model [20–22] a DA of the form

$$\phi_S^B(x) = N_S x(1-x)^3 \exp \left[ -b^2 \left( \frac{m_q^2}{x} + \frac{m_S^2}{1-x} \right) \right] \quad , \quad (2.12)$$

proved to be quite appropriate for the quark-scalar diquark Fock state of octet baryons  $B$ . The origin of the DA, Eq. (2.12), is a nonrelativistic harmonic-oscillator wave function [30]. Therefore the masses appearing in the exponentials have to be considered as constituent masses (330 MeV for light quarks, 580 MeV for light diquarks, strange quarks are 150 MeV heavier than light quarks). The oscillator parameter  $b^2 = 0.248 \text{ GeV}^{-2}$  is chosen in such a way that the full wave function gives rise to a value of 600 MeV for the mean intrinsic transverse momentum of quarks inside a nucleon. Note that the DA, Eq. (2.12), exhibits a flavor dependence due to the masses in the exponential. The exponential in Eq. (2.12) is merely introduced for theoretical purposes (e.g., in order to suppress the soft end-point regions). In the actual data fitting the exponential plays only a minor role. Therefore, the masses and the oscillator parameter are not considered as free parameters but taken from the literature. We stress that the constituent masses do not appear in the hard-scattering amplitudes.

The dynamics of diquarks is governed by their coupling to gluons and photons. With respect to color the diquark behaves like an antiquark. In order that the diquark in combination with a color-triplet quark gives a colorless baryon it has to be in a color antitriplet state. The color part of the quark-diquark wave function [omitted in Eq. (2.2)] is therefore  $\psi_{qD}^{\text{color}} = (1/\sqrt{3}) \sum_{a=1}^3 \delta_{a\bar{a}}$ . The Feynman rules of electromagnetically interacting scalar diquarks are just those of standard scalar electrodynamics [31]. Replacement of the electric charge  $e_0 e_S$  by  $-g_s t^a$ , with  $g_s = \sqrt{4\pi\alpha_s}$  denoting the strong-coupling constant and  $t^a = \lambda^a/2$  Gell-Mann color matrices, yields the corresponding Feynman rules for strongly interacting scalar diquarks. The explicit expressions for  $\gamma$ -S and  $g$ -S vertices read

$$\begin{aligned} S\gamma S: & -ie_0 e_S (p_1 + p_2)_\mu, & \gamma S g S: & -2ie_0 e_S g_s t^a g_{\mu\nu}, \\ Sg S: & ig_s t^a (p_1 + p_2)_\mu, & g S g S: & ig_s^2 \{t^a, t^b\} g_{\mu\nu}. \end{aligned} \quad (2.13)$$

During the calculation of Feynman diagrams diquarks are treated as pointlike particles. The composite nature of diquarks is taken into account by multiplying the expressions for the various Feynman diagrams with diquark form factors

$$F_S^{(n+2)}(Q^2) = \delta_S \frac{Q_S^2}{Q_S^2 + Q^2} \begin{cases} 1, & n=1, \\ a_S, & n \geq 2, \end{cases} \quad (2.14)$$

which depend on the number ( $n$ ) of gauge bosons going to the diquark. This choice of the form factors ensures that the scaling behavior of the diquark model goes over into that of the pure quark model in the limit  $p_\perp \rightarrow \infty$ . The factor  $\delta_S = \alpha_s(Q^2)/\alpha_s(Q_S^2)$  ( $\delta_S = 1$  for  $Q^2 \leq Q_S^2$ ) provides the correct powers of  $\alpha_s(Q^2)$  for asymptotically large  $Q^2$ . For the running coupling constant  $\alpha_s$ , the one-loop result  $\alpha_s = 12\pi/25 \ln(Q^2/\Lambda_{\text{QCD}}^2)$  is used with  $\Lambda_{\text{QCD}} = 200 \text{ MeV}$ . In addition,  $\alpha_s$  is restricted to be smaller than 0.5. The possibility of diquark excitation and breakup in intermediate states where diquarks can be far off shell is taken into consideration by means of the strength parameter  $a_S$ .

For reasons already mentioned, vector diquarks do not show up in the reactions we are investigating in the present

paper. However, they have been dealt with in Refs. [20–22] to which we refer for further details of the diquark model.

### III. PHOTOPRODUCTION OF MESONS: KINEMATICS AND HELICITY AMPLITUDES

Exclusive photoproduction of pseudoscalar mesons can, in general, be described by four independent helicity amplitudes. Following the notation of Ref. [32] we denote these amplitudes by

$$\begin{aligned} N &= M_{0,-1/2,+1,+1/2}, & S_1 &= M_{0,-1/2,+1,-1/2}, \\ D &= M_{0,+1/2,+1,-1/2}, & S_2 &= M_{0,+1/2,+1,+1/2}. \end{aligned} \quad (3.1)$$

$N$ ,  $S_1$ ,  $S_2$ , and  $D$  represent nonflip, single-flip, and double-flip amplitudes, respectively. Our helicity amplitudes are normalized in such a way that the unpolarized differential cross section is given by

$$\frac{d\sigma}{dt} = \frac{1}{32\pi(s-m_p^2)^2} (|N|^2 + |S_1|^2 + |S_2|^2 + |D|^2). \quad (3.2)$$

As we have argued above, two of the four amplitudes vanish,  $N=D=0$ , if we concentrate on the particular process  $\gamma p \rightarrow K^+ \Lambda$  and treat it within the diquark model. Out of the 15 polarization observables discussed in Ref. [32] there are only 3 observables which remain nonzero and which differ from each other (and from  $d\sigma/dt$ ) for vanishing  $N$  and  $D$ . These can be chosen as the photon asymmetry

$$\Sigma \frac{d\sigma}{dt} = \frac{d\sigma_{\perp}}{dt} - \frac{d\sigma_{\parallel}}{dt} = \frac{1}{16\pi(s-m_p^2)^2} \text{Re}(S_1^* S_2 - ND^*), \quad (3.3)$$

and the two double-polarization observables

$$G \frac{d\sigma}{dt} = - \frac{1}{16\pi(s-m_p^2)^2} \text{Im}(S_1 S_2^* + ND^*), \quad (3.4)$$

and

$$E \frac{d\sigma}{dt} = \frac{1}{32\pi(s-m_p^2)^2} (|N|^2 - |S_1|^2 + |S_2|^2 - |D|^2). \quad (3.5)$$

$d\sigma_{\perp}$  ( $d\sigma_{\parallel}$ ) denotes the cross section for photons polarized perpendicular (parallel) to the reaction plane.

Photoproduction of vector mesons may be expressed by altogether 12 linear independent helicity amplitudes [33]. The diquark model leaves four amplitudes nonzero if applied to the formation of the  $K^{*+} \Lambda$  final state. In addition to  $S_1$  and  $S_2$  one can choose, e.g.,  $M_{+1,-1/2,+1,+1/2}$  and  $M_{-1,+1/2,+1,-1/2}$ . Because of the lack of experimental data we will restrict our discussion of  $K^{*+} \Lambda$  production to the unpolarized differential cross section which is obtained from Eq. (3.2) by including also  $|M_{+1,-1/2,+1,+1/2}|^2$  and  $|M_{-1,+1/2,+1,-1/2}|^2$ .

The hard-scattering amplitude  $\hat{T}_{\{\lambda\}}$  for the elementary process  $\gamma u S_{[u,d]} \rightarrow u \bar{s} S_{[u,d]}$  consists, in general, of 79 different tree diagrams. However, only 63 diagrams are encountered if the outgoing meson is a  $K^+$  or  $K^{*+}$ . The other 16

diagrams require the  $s\bar{s}$  pair to go into the produced meson. Diagrams of this type would, e.g., be important in  $\gamma p \rightarrow \phi p$ .

The helicity structure of the hard-scattering amplitude  $\hat{T}_{\{\lambda\}}$  is particularly simple for the  $K^+ \Lambda$  and  $K^{*+} \Lambda$  final states. Assigning helicity labels to the hadronic constituents as in Fig. 1 one finds (with the  $S$  diquark helicities  $\lambda_2 = \lambda_6 = 0$ ):

$$\begin{aligned} \lambda_p &= \lambda_1 = \lambda_3, \\ \lambda_{\Lambda} &= \lambda_5 = -\lambda_4. \end{aligned} \quad (3.6)$$

Thus the quark helicities are uniquely determined by the proton and  $\Lambda$  helicity, respectively. The additional relation (hadronic helicity conservation)

$$\lambda_3 + \lambda_4 = \lambda_p - \lambda_{\Lambda} = \lambda_{K^{(*)}} \quad (3.7)$$

is the condition for the hard-scattering amplitude  $\hat{T}_{\{\lambda\}}$  and consequently the hadronic amplitude  $M_{\{\lambda\}}$  to become nonzero within the diquark model.

As depicted in Fig. 2, the hard-scattering amplitude  $\hat{T}_{\{\lambda\}}(x_1, y_1, z_1; \hat{s}, \hat{t})$  for the elementary process  $\gamma u S_{[u,d]} \rightarrow u \bar{s} S_{[u,d]}$  can be decomposed into three-, four-, and five-point contributions

$$\begin{aligned} \hat{T}_{\{\lambda\}}(x_1, y_1, z_1; \hat{s}, \hat{t}) &= -\frac{2}{\sqrt{6}} e_u [\hat{T}_{\{\lambda\}}^{(3,q)}(x_1, y_1, z_1; \hat{s}, \hat{t}) \\ &\quad + \hat{T}_{\{\lambda\}}^{(4,q)}(x_1, y_1, z_1; \hat{s}, \hat{t}) \\ &\quad - \frac{2}{\sqrt{6}} e_s [\hat{T}_{\{\lambda\}}^{(3,\bar{q})}(x_1, y_1, z_1; \hat{s}, \hat{t}) \\ &\quad + \hat{T}_{\{\lambda\}}^{(4,\bar{q})}(x_1, y_1, z_1; \hat{s}, \hat{t}) \\ &\quad - \frac{2}{\sqrt{6}} e_{ud} [\hat{T}_{\{\lambda\}}^{(4,S)}(x_1, y_1, z_1; \hat{s}, \hat{t}) \\ &\quad + \hat{T}_{\{\lambda\}}^{(5,S)}(x_1, y_1, z_1; \hat{s}, \hat{t})], \end{aligned} \quad (3.8)$$

depending on whether one, two, or three gauge bosons go to the diquark. The additional superscripts  $q$ ,  $\bar{q}$ , and  $S$  occurring in Eq. (3.8) indicate whether the photon couples to the  $u$  quark, the  $s$  quark, or the  $S$  diquark, respectively. For the numerical evaluation of the convolution integral, Eq. (2.1) it is advantageous to further subdivide the various  $n$ -point contributions into two parts which differ by their propagator singularities:

$$\begin{aligned} \hat{T}_{\{\lambda\}}^{(3,q)}(x_1, y_1, z_1; \hat{s}, \hat{t}) &= \frac{f_{\{\lambda\}}^{(3,q)}(x_1, y_1, z_1; \hat{s}, \hat{t})}{(q_2^2 + i\epsilon)(g_1^2 + i\epsilon')} \\ &\quad + \frac{g_{\{\lambda\}}^{(3,q)}(x_1, y_1, z_1; \hat{s}, \hat{t})}{(q_3^2 + i\epsilon)(q_4^2 + i\epsilon')}, \end{aligned}$$

$$\begin{aligned}
\hat{T}_{\{\lambda\}}^{(3,\bar{q})}(x_1, y_1, z_1; \hat{s}, \hat{t}) &= \frac{f_{\{\lambda\}}^{(3,\bar{q})}(x_1, y_1, z_1; \hat{s}, \hat{t})}{(q_2^2 + i\epsilon)(q_5^2 + i\epsilon')} \\
&\quad + \frac{g_{\{\lambda\}}^{(3,\bar{q})}(x_1, y_1, z_1; \hat{s}, \hat{t})}{(q_3^2 + i\epsilon)(g_3^2 + i\epsilon')}, \\
\hat{T}_{\{\lambda\}}^{(4,q)}(x_1, y_1, z_1; \hat{s}, \hat{t}) &= \frac{f_{\{\lambda\}}^{(4,q)}(x_1, y_1, z_1; \hat{s}, \hat{t})}{(g_1^2 + i\epsilon)(D_1^2 + i\epsilon')} \\
&\quad + \frac{g_{\{\lambda\}}^{(4,q)}(x_1, y_1, z_1; \hat{s}, \hat{t})}{(g_1^2 + i\epsilon)}, \\
\hat{T}_{\{\lambda\}}^{(4,\bar{q})}(x_1, y_1, z_1; \hat{s}, \hat{t}) &= \frac{f_{\{\lambda\}}^{(4,\bar{q})}(x_1, y_1, z_1; \hat{s}, \hat{t})}{(g_3^2 + i\epsilon)(D_2^2 + i\epsilon')} \\
&\quad + \frac{g_{\{\lambda\}}^{(4,\bar{q})}(x_1, y_1, z_1; \hat{s}, \hat{t})}{(g_3^2 + i\epsilon)}, \\
\hat{T}_{\{\lambda\}}^{(4,S)}(x_1, y_1, z_1; \hat{s}, \hat{t}) &= \frac{f_{\{\lambda\}}^{(4,S)}(x_1, y_1, z_1; \hat{s}, \hat{t})}{(q_5^2 + i\epsilon)(g_2^2 + i\epsilon')} \\
&\quad + \frac{g_{\{\lambda\}}^{(4,S)}(x_1, y_1, z_1; \hat{s}, \hat{t})}{(q_4^2 + i\epsilon)(g_2^2 + i\epsilon')}, \\
\hat{T}_{\{\lambda\}}^{(5,S)}(x_1, y_1, z_1; \hat{s}, \hat{t}) &= \frac{f_{\{\lambda\}}^{(5,S)}(x_1, y_1, z_1; \hat{s}, \hat{t})}{(D_1^2 + i\epsilon)(D_2^2 + i\epsilon')} \\
&\quad + \frac{g_{\{\lambda\}}^{(5,S)}(x_1, y_1, z_1; \hat{s}, \hat{t})}{(g_2^2 + i\epsilon)}. \quad (3.9)
\end{aligned}$$

Apart from  $g_3^{-2}$  the  $q_i^{-2}$ ,  $D_i^{-2}$ , and  $g_i^{-2}$  denote just those quark, diquark, and gluon propagators which can go on shell when integrating over  $x_1$ ,  $y_1$ , and  $z_1$ . In order to make symmetry properties of the functions  $f$  and  $g$  with respect to interchange of Mandelstam variables and momentum fractions more obvious (cf. Appendix A) we have also extracted the nonsingular gluon propagator  $g_3^{-2}$ . Explicitly the propagator denominators read

$$\begin{aligned}
q_2^2 &= y_2 z_2 \hat{s} + x_2 y_2 \hat{t} + x_2 z_2 \hat{u}, & g_1^2 &= z_2 \hat{s} + x_2 \hat{t} + x_2 z_2 \hat{u}, \\
q_3^2 &= y_2 z_1 \hat{s} + x_2 y_2 \hat{t} + x_2 z_1 \hat{u}, & g_2^2 &= y_1 \hat{s} + x_1 y_1 \hat{t} + x_1 \hat{u}, \\
q_4^2 &= y_1 z_2 \hat{s} + x_1 y_1 \hat{t} + x_1 z_2 \hat{u}, & g_3^2 &= y_2 z_1 \hat{s} + y_2 \hat{t} + z_1 \hat{u}, \\
q_5^2 &= y_1 z_1 \hat{s} + x_1 y_1 \hat{t} + x_1 z_1 \hat{u}, & D_1^2 &= y_1 z_2 \hat{s} + x_2 y_1 \hat{t} + x_2 z_2 \hat{u}, \\
D_2^2 &= y_2 z_1 \hat{s} + x_1 y_2 \hat{t} + x_1 z_1 \hat{u}. \quad (3.10)
\end{aligned}$$

As already indicated in Eq. (3.9), propagator singularities are treated by means of the usual  $i\epsilon$  prescription.

Analytical expressions for the functions  $f$  and  $g$  (cf. Appendix A) have been derived with the help of ‘‘FEYNARTS’’ [34] and ‘‘FEYNALC’’ [35], two program packages written in ‘‘Mathematica’’ which serve the automatic generation and evaluation of Feynman diagrams. Since ‘‘FEYNARTS’’ only

contains the Feynman rules of the standard model, it had to be extended to deal with  $S$  diquarks as well. The spinor techniques developed by Kleiss and Stirling [36] have been utilized to convert strings of  $\gamma$  matrices sandwiched between spinors into traces which can be handled by FEYNALC. A strong indication for the correctness of our results is already the agreement (apart from a detected sign error) with a previous independent calculation [37] performed with FORM [38] (another symbolic computer program for high-energy physics). Further checks of our analytical results were carried out by testing the  $U(1)$  gauge invariance with respect to the photon and the  $SU(3)$  gauge invariance with respect to the gluon. The proof of gauge invariance is facilitated by observing that not only the sum of all 63 tree diagrams gives a gauge invariant expression, but rather each of the functions  $f$  and  $g$  in Eq. (3.9) is by itself gauge invariant. In addition to the gauge invariance tests, a few diagrams were recalculated by hand.

#### IV. NUMERICAL RESULTS

Our numerical studies are performed with the set of diquark-model parameters

$$f_S = 73.85 \text{ MeV}, \quad Q_S^2 = 3.22 \text{ GeV}^2, \quad a_S = 0.15, \quad (4.1)$$

which has been found by fitting elastic electron-nucleon scattering data [20] and which provides also reasonable results in other applications of the diquark model [21,22]. A detailed explanation how the convolution integral, Eq. (2.1), for the various  $n$ -point contributions has been treated numerically is given in Appendix B. At this point we only want to emphasize that propagator singularities have been carefully separated and integrated analytically. The remaining integrals could be performed by means of rather fast fixed-point Gaussian quadrature.

One of the characteristic qualitative features of perturbative QCD predictions is the fixed-angle scaling behavior of cross sections. Within the diquark model the  $\gamma p \rightarrow K^{(*)+} \Lambda$  cross section behaves at large  $\hat{s}$  like

$$\frac{d\sigma}{dt} \propto \hat{s}^{-5} [F_S^{(3)}(-\langle x_2 \rangle \langle y_2 \rangle \hat{t})]^2 h(\hat{t}/\hat{s}) \underset{\hat{s} \rightarrow \infty}{\sim} \hat{s}^{-7} \tilde{h}(\hat{t}/\hat{s}). \quad (4.2)$$

$\langle x_2 \rangle$  and  $\langle y_2 \rangle$  denote average values of the longitudinal momentum fraction of the diquark in a proton or  $\Lambda$ , respectively. Equation (4.2) shows that the scaling behavior of the pure quark hard-scattering model [10] is recovered in the limit  $\hat{s} \rightarrow \infty$ . However, at finite  $\hat{s}$ , where the diquark form factor  $F_S^{(3)}$  becomes operational and diquarks appear as nearly elementary particles, the  $\hat{s}^{-7}$  power law is modified. Additional deviations from the  $\hat{s}^{-7}$  decay of the cross section are due to logarithmic corrections (hidden in the functions  $F_S^{(3)}$  and  $h$ ) which have their origin in the running coupling constant  $\alpha_s$  and eventually in the evolution of the DA’s  $\phi$  (neglected in our calculation).

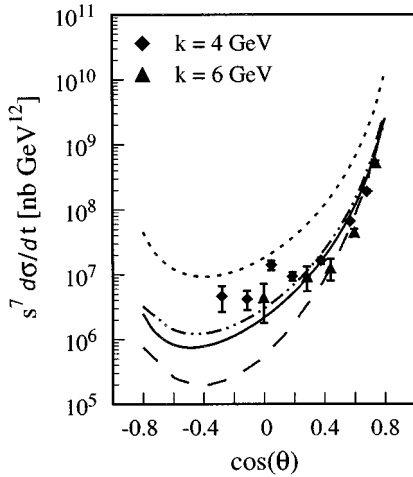


FIG. 3. Differential cross section for  $\gamma p \rightarrow K^+ \Lambda$  scaled by  $s^7$  vs  $\cos(\theta_{c.m.})$ . Solid (dash-double-dotted) line: diquark-model result at  $p_{lab}^\gamma = 6$  GeV (4 GeV), proton and lambda DA's chosen according to Eq. (2.12), kaon DA according to Eq. (2.8) (asymptotic DA); short-dashed line: diquark-model result at  $p_{lab}^\gamma = 6$  GeV, proton and lambda DA's chosen according to Eq. (2.12), kaon DA according to Eq. (2.9) (Chernyak-Zhitnitsky DA [11]); long-dashed line: quark-model result [19] for the asymmetric proton and lambda DA's of Ref. [12] and the kaon DA, Eq. (2.9). Experimental data are taken from Ref. [39].

#### A. $\gamma p \rightarrow K^+ \Lambda$

Figure 3 shows the diquark-model predictions for  $s^7 d\sigma/dt$  along with the few existing large-momentum transfer data [39] and the outcome of the pure quark hard-scattering model [19] (long-dashed curve). Whereas the DA's of proton and  $\Lambda$  have been kept fixed according to Eq. (2.12) we have varied the  $K^+$  DA. The solid and the short-dashed line represent results for the asymptotic [Eq. (2.8)] and the two-humped [Eq. (2.9)]  $K^+$  DA, respectively, evaluated at  $E_{lab}^\gamma = 6$  GeV. The better performance of the asymptotic DA and the overshooting of the asymmetric DA is in line with the conclusion drawn from the investigation of the pion-photon transition form factor [15,40] where, for the case of the pion, the Chernyak-Zhitnitsky (CZ) DA is clearly ruled out. There, strongly end-point concentrated DA's are also overshooting the data. Our findings have to be contrasted with those obtained within the pure quark-model calculation of photoproduction [19], where the asymptotic forms for both, baryon and meson DA's, give systematically larger results than the combination of very asymmetric DA's. However, the numerics of Ref. [19] must be taken with some proviso. For Compton scattering off nucleons it has been demonstrated [41] that the very crude treatment of propagator singularities adopted in Ref. [19], namely keeping  $i\epsilon$  small but finite, may lead to deviations from the correct result which are as large as 1 order of magnitude. The sensitivity of our calculation to the choice of the baryon DA's has been checked only with respect to their end-point behavior  $x \rightarrow 0, 1$ . Neglecting the exponential factor in Eq. (2.12) results in a slight reduction of the cross section, e.g.,  $\approx 8\%$  at  $\theta_{c.m.} = 90^\circ$  and  $E_{lab}^\gamma = 6$  GeV. Deviations from the scaling behavior can be estimated by comparing the dash-double-

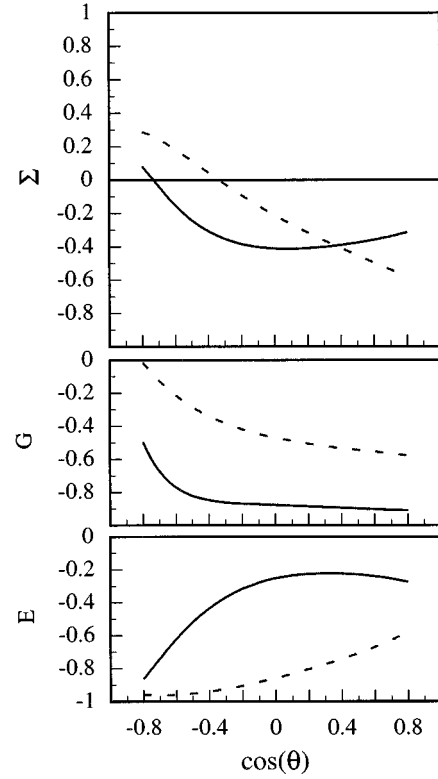


FIG. 4. Diquark model predictions for the nonvanishing  $\gamma p \rightarrow K^+ \Lambda$  polarization observables. Solid (short-dashed) line: same as in Fig. 3.

dotted and the solid curve, which correspond to the asymptotic  $K^+$  DA at  $E_{lab}^\gamma = 4$  and 6 GeV, respectively.

We have also examined the relative importance of various groups of Feynman graphs and found the three-point contributions to be by far the most important. Four- and five-point contributions amount to  $\approx 5\%$  at  $\theta_{c.m.} = 90^\circ$  and  $E_{lab}^\gamma = 6$  GeV as long as only  $d\sigma/dt$  is considered. Their influence decreases from larger to smaller angles. Spin observables, on the other hand, are much more affected by four- and five-point contributions.

The three nonvanishing spin observables  $E$ ,  $\Sigma$ , and  $G$  are depicted in Fig. 4. Whereas  $E$  measures the relative strength of the two amplitudes  $S_1$  and  $S_2$ ,  $\Sigma$  and  $G$  are in addition influenced by the phase difference of these two amplitudes. To make the interplay of the two amplitudes  $S_1$  and  $S_2$  more obvious we have also plotted their moduli and phases in Figs. 5 and 6, respectively. For both choices of the kaon DA  $S_1$  is observed to be the dominant amplitude in backward direction. For  $\phi_{CZ}^K$  it remains dominant over the whole angular range. In contrast,  $S_2$  becomes increasingly important for  $\phi_{asy}^K$  if one goes from backward to forward direction. This behavior is clearly reflected by the double-polarization observable  $E$ . The phase difference between  $S_1$  and  $S_2$  varies rather moderately over the whole angular range for  $\phi_{asy}^K$ , whereas it changes dramatically for  $\phi_{CZ}^K$ . Unfortunately, the information on the phase difference is hidden in the photon asymmetry  $\Sigma$  and the double polarization observable  $G$  for which the dependence on the choice of the kaon DA is not so aggravating.

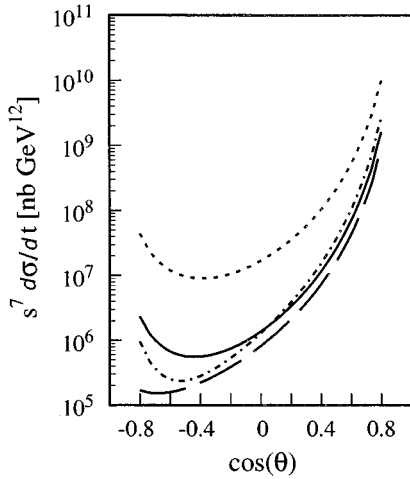


FIG. 5. Differential cross section for  $\gamma p \rightarrow K^+ \Lambda$  scaled by  $s^7$  vs  $\cos(\theta_{c.m.})$  at  $p_{lab}^\gamma = 6$  GeV, contributions of the helicity amplitudes  $S_1$  and  $S_2$ , respectively. Solid (long-dashed) line: contribution of  $S_1$  ( $S_2$ ) for proton and lambda DA's chosen according to Eq. (2.12), kaon DA according to Eq. (2.8); short-dashed (dash-dotted) line: contribution of  $S_1$  ( $S_2$ ) for proton and lambda DA's chosen according to Eq. (2.12), kaon DA according to Eq. (2.9).

Let us recall at this point that the occurrence of nontrivial phases in photoproduction amplitudes is a consequence of the fact that most of the Feynman diagrams contain internal gluons that can propagate on mass shell in certain kinematic regions of the momentum-fraction space. The treatment of the corresponding propagator singularities by means of the usual Feynman prescription results in an imaginary contribution to photoproduction amplitudes. One may worry about the validity of perturbation theory for a freely propagating gluon which is expected to be modified by long-distance effects. But fortunately photoproduction belongs to a class of exclusive reactions which does, to leading-order perturbative QCD, not require the resummation of gluonic radiative corrections (Sudakov effects). As has been proved in Ref. [42], the standard factorization formula, Eq. (2.1), produces already an infrared finite amplitude.

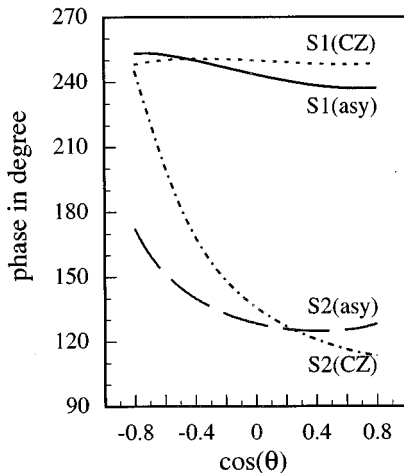


FIG. 6. Phases of the helicity amplitudes  $S_1$  and  $S_2$ , respectively. Lines as in Fig. 5.

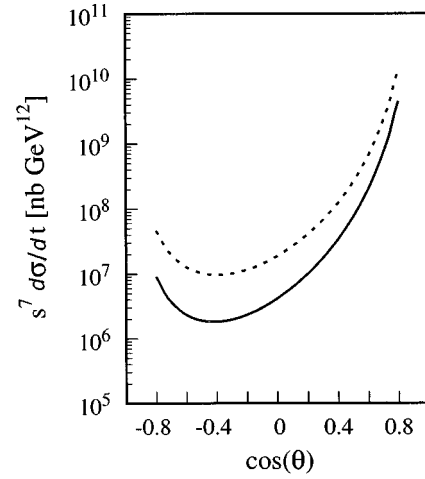


FIG. 7. Differential cross section for  $\gamma p \rightarrow K^{*+} \Lambda$  scaled by  $s^7$  vs  $\cos(\theta_{c.m.})$  at  $p_{lab}^\gamma = 6$  GeV. Solid line: diquark-model prediction, proton and lambda DA's chosen according to Eq. (2.12),  $K^*$  DA according to Eq. (2.8) (asymptotic DA); short-dashed line: diquark-model prediction, proton and lambda DA's chosen according to Eq. (2.12),  $K^*$  DA according to Eqs. (2.10) and (2.11) (taken from Ref. [28]).

Unlike  $\Sigma$ ,  $G$ , and  $E$ , which have not been measured as yet, the determination of the  $\Lambda$  polarization  $P$  has been attempted already [43] (for more recent efforts, cf. Ref. [6]). The way to determine the transverse polarization of the  $\Lambda$  is to detect, in addition to the  $K^+$ , the proton coming from the weak  $\Lambda \rightarrow p \pi^-$  decay. The transverse  $\Lambda$  polarization  $P$  then follows from the known ( $P$ -dependent) angular distribution of the weak  $\Lambda \rightarrow p \pi^-$  decay. According to the diquark model, and also the pure quark model,  $P$  is expected to vanish in the hard-scattering regime ( $tu/s \gg m_p^2$ ). The present data, however, are at too small  $s$  and  $t$  to allow conclusions about the validity and quality of these perturbative models. It would be interesting to see, whether the occurrence of sizable transverse polarizations at  $p_\perp \approx$  few GeV, as observed, e.g., in elastic  $p$ - $p$  scattering [44] or inclusive production of hyperons in  $p$ - $p$  collisions [45], continues to the  $\gamma p \rightarrow K^+ \Lambda$  process. This would be an indication that, besides the perturbative mechanism, non-perturbative physics (beyond diquarks) is still at work.

We have also computed differential cross sections for the reaction  $\gamma n \rightarrow K^0 \Lambda$ . For  $\cos(\theta_{c.m.}) \geq 0$  they are considerably smaller than the corresponding  $\gamma p \rightarrow K^+ \Lambda$  cross sections. The amount of suppression depends on the choice of the  $K^0$  DA. For the asymptotic DA the suppression factor is  $\approx 10$  in the whole forward region, whereas it increases for the two-humped DA from 2 to  $\approx 10$  when  $\cos(\theta_{c.m.})$  is varied from 0 to 0.8 ( $E_{lab}^\gamma = 6$  GeV). In view of the plans at CEBAF to study  $\gamma n \rightarrow K^0 \Lambda$  by means of a deuteron target [5] this is certainly an interesting observation which could be helpful to pin down the uncertainties of the kaon DA.

## B. $\gamma p \rightarrow K^{*+} \Lambda$

The diquark-model results for  $(d\sigma/dt)_{\gamma p \rightarrow K^{*+} \Lambda}$  are plotted in Fig. 7. Again curves are shown for two choices of the

$K^{*+}$  DA with  $p$  and  $\Lambda$  DA kept fixed ( $E_{\text{lab}}^\gamma = 6$  GeV). The results resemble those for photoproduction of  $K^+$  mesons. Cross sections for the asymmetric DA, Eqs. (2.10) and (2.11), are nearly 1 order of magnitude larger than for the asymptotic DA, Eq. (2.8). If  $\phi_{\text{asy}}$  is taken for both,  $K^+$  and  $K^{*+}$ , the photoproduction cross section for the  $K^{*+}$  vector meson is found to be by a factor of 1.8–3.6 (depending on the scattering angle) larger than that for the pseudoscalar  $K^+$  meson. An increase by a factor 1.73 is due to the different  $K^+$  and  $K^{*+}$  decay constants  $f^K$  and  $f^{K^*}$ . The remaining difference is caused by the contribution of transversially polarized  $K^{*+}$  mesons, which increases from small to large scattering angles. The situation would be quite similar if we had taken  $\phi_{\text{CZ}}^K$  for both,  $K^+$  and  $K^{*+}$ . However, the enhancement of the  $K^{*+}$  cross section is completely compensated, if  $\phi_{\text{CZ}}^K$  is replaced by  $\phi_L^{K^*}$  and  $\phi_T^{K^*}$  [cf. Eqs. (2.10) and (2.11)] when going from  $K^+$  to  $K^{*+}$  photoproduction.

Until now large momentum-transfer data for photoproduction of vector mesons are only available for the reaction  $\gamma p \rightarrow (\rho_0 + \omega)p$  [39]. At  $\theta_{\text{c.m.}} = 90^\circ$  and  $E_{\text{lab}}^\gamma \approx 6$  GeV the experimental value of the cross section ratio  $(d\sigma/dt)_{\gamma p \rightarrow (\rho_0 + \omega)p} / (d\sigma/dt)_{\gamma p \rightarrow \pi_0 p}$  is  $\approx 2$ . This means in particular that  $(d\sigma/dt)_{\gamma p \rightarrow \rho_0 p} \lesssim 2(d\sigma/dt)_{\gamma p \rightarrow \pi_0 p}$ . The difference in the  $\rho_0$  and  $\pi_0$  decay constants ( $f_{\text{decay}}^\rho \approx 1.5f_{\text{decay}}^\pi$ ), however, already implies an enhancement of the  $\rho_0$  photoproduction cross section as compared to the  $\pi_0$  one by a factor of  $\approx 2.3$  which is further magnified by contributions of transversially polarized  $\rho$ 's. The only way to compensate part of this enhancement is to assume that (as above in the case of  $K^+$  and  $K^{*+}$ ) the DA's of  $\pi$  and  $\rho$  differ from each other. Experimental data on photoproduction of pseudoscalar and vector mesons with the same flavor content could thus be very useful to work out differences in the corresponding DA's.

## V. SUMMARY AND CONCLUSIONS

We have investigated photoproduction of  $K$ - $\Lambda$  and  $K^*$ - $\Lambda$  final states in the few-GeV momentum-transfer region. Our analysis is based on perturbative QCD supplemented by the assumption that baryons can be treated as quark-diquark systems. The present calculation continues previous work on photon-induced hadronic reactions [20–22] performed within the same approach. By modeling quark-quark correlations inside a baryon as quasi-elementary particles—scalar and vector diquarks—we account for some nonperturbative effects. In this way we are able to extend the range of applicability of the pure quark hard-scattering approach (HSA) from large down to moderately large momentum transfers. The fact that the photoproduction channels we are interested in contain a  $\Lambda$  in the final state entails a considerable reduction in computational effort. In contrast to arbitrary photoproduction reactions only scalar diquarks must be taken into consideration. This has the consequence that helicity amplitudes and hence spin observables violating hadronic helicity

conservation [cf. Eq. (3.7)], e.g., the  $\Lambda$  polarization, are predicted to vanish.

Our numerical studies have been performed with the diquark-model parameters and the quark-diquark DA's proposed in Ref. [20]. We have paid special attention to the correct and numerically robust treatment of propagator singularities (cf. Appendix B). Reasonable agreement with the few existing  $\gamma p \rightarrow K^+ \Lambda$  data is achieved already with the asymptotic form for the  $K^+$  DA. On the other hand, the end-point concentrated  $K^+$  DA, based on QCD sum rules [11], seems to perform less well. The corresponding curve lies far beyond the data. The difference between these two kaon DA's is also clearly visible in the three nonvanishing polarization observables, i.e., the photon asymmetry  $\Sigma$  and the two double-polarization observables  $G$  and  $E$ . It is most pronounced in the observable  $E$ . Another quantity which we found to be very sensitive on the choice of the kaon DA is the angular dependence of the cross-section ratio  $(d\sigma/dt)_{\gamma p \rightarrow K^0 \Lambda} / (d\sigma/dt)_{\gamma p \rightarrow K^+ \Lambda}$ . For the photoproduction of the  $K^*$  vector meson there are no data to compare with. We have again tested the asymptotic DA and a  $K^*$  DA which obeys QCD sum-rule constraints on the lowest moments [28]. The differences in the results for the two DA's are quite similar to those for photoproduction of the pseudoscalar  $K^+$  meson. When going from  $K$  to  $K^*$  photoproduction the cross section becomes larger due to the different  $K$  and  $K^*$  decay constants and the additional contributions from transversially polarized  $K^*$ s. This increase of the cross section, however, is partly compensated if different DA's for  $K$  and  $K^*$  are used.

To the best of our knowledge the diquark model is at present the only constituent-scattering model which is able to account for the large- $p_\perp$  photoproduction data of the  $K$ - $\Lambda$  final state. Admittedly, the momentum transfers at which we compare our predictions with experiments are somewhat low for a model based on perturbative QCD. However, we want to point out that we compare with appropriately scaled cross sections. Keeping in mind that the fixed-angle scaling behavior is based on dimensional counting [46], i.e., on much more general grounds than on a particular perturbative model, and assuming that one is close to the scaling region with the experimentally accessible photon energies one would expect that the scaled cross sections stay, apart from logarithmic corrections due to the running  $\alpha_s$ , essentially the same at higher photon energies where perturbative QCD becomes applicable. Similarly, the (scaled) theoretical predictions would not change very much if the calculations were done at higher photon energies (also neglecting the logarithmic  $p_\perp$  dependence of  $\alpha_s$ ). The still remaining slight deviations from the  $s^{-7}$  scaling behavior are, as already mentioned at the beginning of Sec. IV, due to the diquark form factors. That our results for the photoproduction cross section, obtained without adjusting any parameter, agree with the data is an interesting finding which parallels similar successes of the diquark model for Compton scattering [22] and its crossed reaction,  $\gamma\gamma \rightarrow p\bar{p}$  [21].

One may now object that, like in the pure quark hard-scattering approach (see, e.g., Ref. [47]), the perturbative result obtained in collinear approximation is considerably reduced if effects due to the intrinsic transverse momentum are included. In applications of the diquark model to baryon

form factors [20] this question has been investigated in some detail. It turned out, e.g., that Sudakov corrections diminish the result for the proton magnetic form factor  $G_M^p$  by 10–20 %, depending on the momentum transfer. A further reduction by a somewhat smaller percentage is observed if intrinsic transverse momenta are also taken into account in the proton wave function [48]. There are two reasons why Sudakov corrections and transverse-momentum effects are less aggravating in the diquark model than in the pure quark model: On the one hand, the “freezing” of  $\alpha_s$  due to Sudakov corrections is effectively taken into account by the restriction  $\alpha_s \leq 0.5$ ; on the other hand, contributions from the end-point regions  $x \rightarrow 0, 1$  are already strongly damped due to the quark-diquark DA’s [cf. Eq. (2.12)] used, in particular due to the exponential factor.<sup>1</sup> We expect these findings to hold for photoproduction as well. It should also be noted that in photoproduction processes some of the propagators are timelike, in which case the transverse momenta lead to an enhancement of the result. However, we want to point out that even with baryons considered as quark-diquark systems, an explicit calculation of photoproduction within the modified HSA including transverse momentum would be a very demanding task, perhaps impossible to be carried through. The reasons are that the convolution integral of the hard-scattering amplitude with the hadronic wave functions becomes high-dimensional and the numerical tractability of the integrand is in addition complicated by the existence of propagator singularities. Anyway, after having checked for a simple application, like the electromagnetic nucleon form factors, that transverse-momentum effects of altogether 20–40% can be absorbed into the parameters of the diquark model we think that it does not make too much sense to consider such subtleties also for more complicated reactions; this would rather spoil the usefulness of such an approach. An indirect check for the quality and range of applicability of a phenomenological model like ours is rather its ability to describe a large class of exclusive hadronic reactions in a consistent way, i.e., with the same set of parameters and hadron DA’s. Apart from the successful applications mentioned above preliminary results for other photoproduction channels, such as  $\gamma p \rightarrow K^+ \Sigma^0$  and  $\gamma p \rightarrow \pi^+ n$ , look also rather promising [50]. That the leading-order perturbative contribution of the diquark model is already sizable at a few GeV of momentum transfer, even after inclusion of transverse-momentum effects, seems to be surprising in view of opposite conclusions for the pure quark model [16]. One reason is that for a particular process a smaller number of gluons is exchanged as compared to the pure quark model. Hence the perturbative domain is extended down to smaller momentum transfers. The second reason is that part of the soft contributions are modeled by the diquarks. This can even be understood formally. Soft contributions may be estimated by means of the overlap of the (full) wave functions of incoming and outgoing hadrons (see, e.g., Ref. [51] for hadron form factors, and Ref. [9] for more complicated hadronic

processes<sup>2</sup>). By assuming that two quarks make up a diquark part of the multidimensional overlap integral and thus part of the soft contributions can be absorbed into diquark form factors which in our model are parametrized phenomenologically over the whole momentum-transfer range. Adding soft contributions to the diquark model will, as mentioned in the previous footnote, likely lead to some double counting. Formally diquarks, as any other soft contribution (e.g. overlap contributions), represent higher twist effects.

With regard to future experiments we consider, apart from more and better large  $p_\perp$  cross-section data, the polarization measurement of the recoiling  $\Lambda$  as one of the most urgent tasks. A large polarization indicates that the perturbative QCD regime has not been entered yet. In the perturbative QCD regime the kaon DA’s could be restricted by means of quantities, like the photon asymmetry or the cross section ratios  $(d\sigma/dt)_{\gamma n \rightarrow K^0 \Lambda} / (d\sigma/dt)_{\gamma p \rightarrow K^+ \Lambda}$  and  $(d\sigma/dt)_{\gamma p \rightarrow K^* \Lambda} / (d\sigma/dt)_{\gamma p \rightarrow K^+ \Lambda}$ , which are very sensitive to the choice of the DA’s. With a maximal photon laboratory energy of (at present) 4 GeV CEBAF [5] touches at best the border of the hard-scattering domain. More decisive data could be expected from a future electron facility such as ELFE [53] which is designed to explore the energy range up to 15 GeV (or even higher) with a continuous high intensity electron beam.

#### APPENDIX A: ANALYTICAL EXPRESSIONS FOR THE HARD AMPLITUDES

In this appendix we quote analytical expressions for those hard amplitudes which describe the process  $\gamma u S_{[u,d]} \rightarrow u \bar{s} S_{[u,d]}$  with the  $s\bar{s}$  pair being in a spin-zero state. More generally speaking, these are just the scalar diquark contributions to photoproduction of pseudoscalar mesons. According to Eq. (3.9) the various  $n$ -point contributions to these amplitudes can be decomposed into gauge-invariant functions  $f$  and  $g$ . The functions  $f$  and  $g$  which determine the hadronic (helicity conserving) amplitude  $S_1$  read

<sup>2</sup>At this point a few remarks are in order. Whereas the Drell-Yan formula (including contributions from all Fock states) is an exact representation of hadron form factors at any momentum transfer, the quark-interchange model of Ref. [9] is rather a model in the spirit of the Drell-Yan formula which, however, does not correspond to the full nonperturbative result. Thus it is not an appropriate starting point for the leading-order perturbative analysis [52]. This is illustrated, e.g., if one considers exclusive photoproduction of a  $\phi$  meson on a proton. Whereas this reaction proceeds via the hadronic valence Fock states in the HSA, a higher Fock component containing an  $s - \bar{s}$  pair from the sea is needed for the proton in the quark-interchange model. Actually, elastic lepton-hadron scattering is the only exclusive reaction for which an exact nonperturbative representation in terms of the hadronic wave functions is known. As a consequence this is also the only case for which nonperturbative contributions can be clearly separated from the leading-order perturbative result without double-counting problems.

<sup>1</sup>The importance of the exponential factor is demonstrated in Fig. 2 of [49] in the case of the pion form factor.

$$\begin{aligned}
f_{0,-1/2,+1,-1/2}^{(3,q)} &= -C_F^{(1)} A_T^{(S,3)} \frac{z_2 \hat{u}}{y_2 z_1 \hat{t}^2} [y_2 \hat{t} + z_2 \hat{u}] , \\
g_{0,-1/2,+1,-1/2}^{(3,q)} &= -C_F^{(1)} A_T^{(S,3)} \frac{\hat{u}}{x_2 y_1 z_1 \hat{s} \hat{t}^2} [q_4^2 (z_1 \hat{s} + x_2 \hat{t}) - x_2 (x_2 - z_1) \hat{s} \hat{t}] , \\
f_{0,-1/2,+1,-1/2}^{(3,\bar{q})} &= -C_F^{(1)} A_T^{(S,3)} \frac{1}{x_1 x_2 y_1 y_2 z_1 \hat{t}^2 \hat{u}} \{ y_1 y_2^2 z_2 (x_2 - z_2) \hat{t}^3 + y_2 [(y_1 - x_1)(y_1 z_2 + y_2 z_1) z_2 + (x_1 y_1 - z_1^2) x_2 y_1] \hat{t}^2 \hat{u} \\
&\quad + [(y_1 - x_1)(y_2^2 z_1 - x_2 y_1^2) z_2 + (y_1 z_2 - x_2 z_1) x_2 y_1 y_2] \hat{t} \hat{u}^2 + x_2 y_1 (y_2 - x_2) z_1 z_2 \hat{u}^3 \} , \\
g_{0,-1/2,+1,-1/2}^{(3,\bar{q})} &= -C_F^{(1)} A_T^{(S,3)} \frac{\hat{s}}{x_2 y_1 \hat{t}^2} [(x_2 - z_1) y_2 \hat{t} + y_1 z_1 \hat{u}] , \\
f_{0,-1/2,+1,-1/2}^{(4,q)} &= -C_F^{(1)} A_T^{(S,4)} \frac{\hat{u}}{y_1 z_1 \hat{s} \hat{t}} [x_2 y_2 \hat{t} - D_1^2] , \\
g_{0,-1/2,+1,-1/2}^{(4,q)} &= -C_F^{(2)} A_T^{(S,4)} \frac{\hat{u}}{x_2 y_1 y_2 z_1 \hat{s} \hat{t}^2} [y_2 z_2 \hat{s} - x_2 \hat{t} - x_2 z_2 \hat{u}] , \\
f_{0,-1/2,+1,-1/2}^{(4,\bar{q})} &= -C_F^{(1)} A_T^{(S,4)} \frac{1}{x_1 y_1 z_1 \hat{t} \hat{u}} [\hat{s} \hat{t} x_2 y_2^2 + D_2^2 (y_2 \hat{t} - y_1 \hat{u})] , \\
g_{0,-1/2,+1,-1/2}^{(4,\bar{q})} &= C_F^{(2)} A_T^{(S,4)} \frac{1}{x_1 x_2 y_1 y_2 \hat{t}^2} [g_3^2 (y_2 \hat{s} + x_2 \hat{u}) + x_1 y_2 \hat{t} \hat{u}] , \\
f_{0,-1/2,+1,-1/2}^{(4,S)} &= -C_F^{(1)} A_T^{(S,4)} \frac{y_1 z_2 \hat{s}}{x_1 z_1 \hat{u}} \\
g_{0,-1/2,+1,-1/2}^{(4,S)} &= -C_F^{(1)} A_T^{(S,4)} \frac{1}{z_2 \hat{s}} [x_1 \hat{t} + z_2 \hat{s}] , \\
f_{0,-1/2,+1,-1/2}^{(5,S)} &= -C_F^{(1)} A_T^{(S,5)} \frac{y_1 z_2 \hat{s}}{x_1 z_1 \hat{u}} [(D_1^2 + x_2 y_1 \hat{t})(D_2^2 - y_2 \hat{u}) + x_2 y_2 (y_1 - y_2 + z_1) \hat{t} \hat{u}] , \\
g_{0,-1/2,+1,-1/2}^{(5,S)} &= -C_F^{(2)} A_T^{(S,5)} \frac{1}{x_1 y_1 z_1 z_2 \hat{s} \hat{u}} [x_1 \hat{u} + z_2 (x_1 \hat{u} - y_1 \hat{s})] , \tag{A1}
\end{aligned}$$

with

$$C_F^{(1)} = \frac{16}{9\sqrt{3}} , \quad C_F^{(2)} = \frac{1}{\sqrt{3}} , \tag{A2}$$

and

$$A_T^{(S,n)} = 128\pi^2 \sqrt{\pi\alpha\alpha_s^2} (\hat{t}\hat{u}/\hat{s}) \sqrt{-\hat{t}} F_S^{(n)}(-x_2 y_2 \hat{t}) , \tag{A3}$$

where  $\alpha$  denotes the fine-structure constant.

The functions  $f$  and  $g$  contributing to the hadronic amplitude  $S_2$  are obtained from those entering  $S_1$  by interchange

of the Mandelstam variables  $\hat{s} \leftrightarrow \hat{u}$  and the momentum fractions  $x_1 \leftrightarrow y_1$  and  $z_1 \leftrightarrow z_2$ . One finds, in particular,

$$f_{0,+1/2,+1,+1/2}^{(3,q)} = -g_{0,-1/2,+1,-1/2}^{(3,\bar{q})} (\hat{s} \leftrightarrow \hat{u}, x_1 \leftrightarrow y_1, z_1 \leftrightarrow z_2) ,$$

$$g_{0,+1/2,+1,+1/2}^{(3,q)} = -f_{0,-1/2,+1,-1/2}^{(3,\bar{q})} (\hat{s} \leftrightarrow \hat{u}, x_1 \leftrightarrow y_1, z_1 \leftrightarrow z_2) ,$$

$$f_{0,+1/2,+1,+1/2}^{(3,\bar{q})} = -g_{0,-1/2,+1,-1/2}^{(3,q)} (\hat{s} \leftrightarrow \hat{u}, x_1 \leftrightarrow y_1, z_1 \leftrightarrow z_2) ,$$

$$g_{0,+1/2,+1,+1/2}^{(3,\bar{q})} = -f_{0,-1/2,+1,-1/2}^{(3,q)} (\hat{s} \leftrightarrow \hat{u}, x_1 \leftrightarrow y_1, z_1 \leftrightarrow z_2) ,$$

$$f_{0,+1/2,+1,+1/2}^{(4,q)} = -f_{0,-1/2,+1,-1/2}^{(4,\bar{q})} (\hat{s} \leftrightarrow \hat{u}, x_1 \leftrightarrow y_1, z_1 \leftrightarrow z_2) ,$$

$$\begin{aligned}
g_{0,+1/2,+1,+1/2}^{(4,q)} &= -g_{0,-1/2,+1,-1/2}^{(4,\bar{q})}(\hat{s} \leftrightarrow \hat{u}, x_1 \leftrightarrow y_1, z_1 \leftrightarrow z_2), \\
f_{0,+1/2,+1,+1/2}^{(4,\bar{q})} &= -f_{0,-1/2,+1,-1/2}^{(4,q)}(\hat{s} \leftrightarrow \hat{u}, x_1 \leftrightarrow y_1, z_1 \leftrightarrow z_2), \\
g_{0,+1/2,+1,+1/2}^{(4,\bar{q})} &= -g_{0,-1/2,+1,-1/2}^{(4,q)}(\hat{s} \leftrightarrow \hat{u}, x_1 \leftrightarrow y_1, z_1 \leftrightarrow z_2), \\
f_{0,+1/2,+1,+1/2}^{(4,S)} &= -f_{0,-1/2,+1,-1/2}^{(4,S)}(\hat{s} \leftrightarrow \hat{u}, x_1 \leftrightarrow y_1, z_1 \leftrightarrow z_2), \\
g_{0,+1/2,+1,+1/2}^{(4,S)} &= -f_{0,-1/2,+1,-1/2}^{(4,S)}(\hat{s} \leftrightarrow \hat{u}, x_1 \leftrightarrow y_1, z_1 \leftrightarrow z_2), \\
f_{0,+1/2,+1,+1/2}^{(5,S)} &= -f_{0,-1/2,+1,-1/2}^{(5,S)}(\hat{s} \leftrightarrow \hat{u}, x_1 \leftrightarrow y_1, z_1 \leftrightarrow z_2), \\
g_{0,+1/2,+1,+1/2}^{(5,S)} &= -g_{0,-1/2,+1,-1/2}^{(5,S)}(\hat{s} \leftrightarrow \hat{u}, x_1 \leftrightarrow y_1, z_1 \leftrightarrow z_2).
\end{aligned} \tag{A4}$$

The hard amplitudes for photoproduction of longitudinally polarized  $K^*$  mesons are (up to a sign change in  $\hat{T}_{0,-1/2,+1,-1/2}$ ) also determined by these expressions. For photoproduction of transversally polarized  $K^*$  mesons the functions  $f$  and  $g$  are of similar length and shape and can be obtained from the authors on request.

## APPENDIX B: NUMERICAL TREATMENT OF PROPAGATOR POLES

The numerical difficulties in performing the convolution integral Eq. (2.1) are mainly caused by the occurrence of propagator singularities in the range of integration which give rise to a principal value integral

$$\frac{1}{k^2 + i\epsilon} = \wp \left( \frac{1}{k^2} \right) - i\pi \delta(k^2). \tag{B1}$$

In what follows, the four cases to be distinguished will be discussed separately.

### 1. No propagator on shell

The only contribution to the convolution integral Eq. (2.1) exhibiting no propagator singularity is the one corresponding to  $g_{\{\lambda\}}^{(4,\bar{q})}$  [cf. Eq. (3.9)]. In these circumstances the convolution integral is easily performed by means of three-dimensional Gaussian quadrature.

### 2. One propagator on shell

If only one of the propagators goes on shell within the integration region—this happens for  $g_{\{\lambda\}}^{(3,\bar{q})}$ ,  $g_{\{\lambda\}}^{(4,q)}$ ,  $f_{\{\lambda\}}^{(4,\bar{q})}$ , and  $g_{\{\lambda\}}^{(5,S)}$ —the corresponding integrals over  $x_1$  have the general structure

$$I^{(k)}(y_1, z_1) = \int_0^1 dx_1 \frac{h(x_1, y_1, z_1)}{k^2 + i\epsilon}. \tag{B2}$$

In order to simplify notations we have neglected helicity labels and the dependence on the Mandelstam variables  $\hat{s}$  and  $\hat{t}$ . Furthermore, the distribution amplitudes  $\phi^p(x_1)$ ,  $\phi^{\Lambda^\dagger}(y_1)$ , and  $\phi^{K^\dagger}(z_1)$  have been absorbed into the function  $h(x_1, y_1, z_1)$ . The integral  $I^{(k)}$  may be rewritten to give

TABLE I. Propagator-pole positions,  $x_1$  derivatives, and principal value integrals for the singular propagators occurring in Eq. (3.9).

$k^2$	$x_1^{(k)}$	$\frac{\partial k^2}{\partial x_1}$	$\wp \int_0^1 \frac{dx_1}{k^2}$
$g_1^2$	$\frac{z_1 \hat{t}}{\hat{t} + z_2 \hat{u}}$	$-(\hat{t} + z_2 \hat{u})$	$\frac{-1}{\hat{t} + z_2 \hat{u}} \ln \left( \frac{-z_2 \hat{s}}{z_1 \hat{t}} \right)$
$g_2^2$	$\frac{-y_1 \hat{s}}{y_1 \hat{t} + \hat{u}}$	$(y_1 \hat{t} + \hat{u})$	$\frac{-1}{y_1 \hat{t} + \hat{u}} \ln \left( \frac{-y_1 \hat{s}}{y_2 \hat{u}} \right)$
$q_2^2$	$\frac{y_2 z_1 \hat{t} + y_1 z_2 \hat{u}}{y_2 \hat{t} + z_2 \hat{u}}$	$-(y_2 \hat{t} + z_2 \hat{u})$	$\frac{-1}{y_2 \hat{t} + z_2 \hat{u}} \ln \left( \frac{-y_2 z_2 \hat{s}}{y_2 z_1 \hat{t} + y_1 z_2 \hat{u}} \right)$
$q_3^2$	$\frac{y_2 z_2 \hat{t} + y_1 z_1 \hat{u}}{y_2 \hat{t} + z_1 \hat{u}}$	$-(y_2 \hat{t} + z_1 \hat{u})$	$\frac{-1}{y_2 \hat{t} + z_1 \hat{u}} \ln \left( \frac{-y_2 z_1 \hat{s}}{y_2 z_2 \hat{t} + y_1 z_1 \hat{u}} \right)$
$q_4^2$	$\frac{-y_1 z_2 \hat{s}}{y_1 \hat{t} + z_2 \hat{u}}$	$(y_1 \hat{t} + z_2 \hat{u})$	$\frac{-1}{y_1 \hat{t} + z_2 \hat{u}} \ln \left( \frac{-y_1 z_2 \hat{s}}{y_1 z_1 \hat{t} + y_2 z_2 \hat{u}} \right)$
$q_5^2$	$\frac{-y_1 z_1 \hat{s}}{y_1 \hat{t} + z_1 \hat{u}}$	$(y_1 \hat{t} + z_1 \hat{u})$	$\frac{-1}{y_1 \hat{t} + z_1 \hat{u}} \ln \left( \frac{-y_1 z_1 \hat{s}}{y_1 z_2 \hat{t} + y_2 z_1 \hat{u}} \right)$
$D_1^2$	$\frac{y_1 z_1 \hat{t} + y_2 z_2 \hat{u}}{y_1 \hat{t} + z_2 \hat{u}}$	$-(y_1 \hat{t} + z_2 \hat{u})$	$\frac{-1}{y_1 \hat{t} + z_2 \hat{u}} \ln \left( \frac{-y_1 z_2 \hat{s}}{y_1 z_1 \hat{t} + y_2 z_2 \hat{u}} \right)$
$D_2^2$	$\frac{-y_2 z_1 \hat{s}}{y_2 \hat{t} + z_1 \hat{u}}$	$(y_2 \hat{t} + z_1 \hat{u})$	$\frac{-1}{y_2 \hat{t} + z_1 \hat{u}} \ln \left( \frac{-y_2 z_1 \hat{s}}{y_2 z_2 \hat{t} + y_1 z_1 \hat{u}} \right)$

$$\begin{aligned}
I^{(k)}(y_1, z_1) &= \int_0^1 dx_1 \frac{h(x_1, y_1, z_1) - h(x_1^{(k)}, y_1, z_1)}{k^2} \\
&\quad + h(x_1^{(k)}, y_1, z_1) \left( \wp \int_0^1 \frac{dx_1}{k^2} - i\pi \left| \frac{\partial k^2}{\partial x_1} \right|^{-1} \right),
\end{aligned} \tag{B3}$$

where  $x_1^{(k)} = x_1^{(k)}(y_1, z_1)$  represents the zero of  $k^2$  (considered as a function of  $x_1$ ). The first integral in Eq. (B3) is now again tractable by simple Gaussian quadrature, whereas the principal-value integral can be done analytically. Since  $I^{(k)}$  is a regular function of  $y_1$  and  $z_1$  Gaussian integration can also be applied to these variables. Analytical expressions for propagator-pole positions, principal value integrals and  $x_1$  derivatives of propagator denominators are listed in Table I.

### 3. Two propagators on shell—propagator poles not coinciding

If two propagators  $k_1^{-2}$  and  $k_2^{-2}$  go on shell one can proceed similarly as in the one-pole case, provided the zeroes  $x_1^{(k_1)} = x_1^{(k_1)}(y_1, z_1)$  and  $x_1^{(k_2)} = x_1^{(k_2)}(y_1, z_1)$  of  $k_1^2$  and  $k_2^2$  (considered as functions of  $x_1$ ) do not coincide for fixed  $y_1$  and  $z_1$ ,  $0 < y_1, z_1 < 1$  arbitrary. This is guaranteed for the Feynman diagrams contributing to  $f_{\{\lambda\}}^{(3,q)}$ ,  $f_{\{\lambda\}}^{(4,q)}$ ,  $f_{\{\lambda\}}^{(4,S)}$ , and  $g_{\{\lambda\}}^{(4,S)}$ . The  $x_1$  integrals to be considered have the general form

$$I^{(k_1, k_2)}(y_1, z_1) = \int_0^1 dx_1 \frac{h(x_1, y_1, z_1)}{(k_1^2 + i\epsilon)(k_2^2 + i\epsilon')} . \quad (\text{B4})$$

If  $x_1^{(k_1)} \neq x_1^{(k_2)}$  a partial fractioning yields

$$I^{(k_1, k_2)}(y_1, z_1) = \frac{1}{x_1^{(k_1)} - x_1^{(k_2)}} \left\{ \left( \frac{\partial k_2^2}{\partial x_1} \right)^{-1} I^{(k_1)}(y_1, z_1) - \left( \frac{\partial k_1^2}{\partial x_1} \right)^{-1} I^{(k_2)}(y_1, z_1) \right\} , \quad (\text{B5})$$

i.e., two terms which again can be treated according to Eq. (B3).

#### 4. Two propagators on shell—propagator poles coinciding

This is the worst case and shows up in connection with the functions  $g_{\{\lambda\}}^{(3,q)}$ ,  $f_{\{\lambda\}}^{(3,\bar{q})}$ , and  $f_{\{\lambda\}}^{(5,S)}$ . The general structure of the  $x_1$  integrals is again that of Eq. (B4). However, now it happens that the two propagator singularities  $x_1^{(k_1)}$  and  $x_1^{(k_2)}$  (which still depend on  $y_1$  and  $z_1$ ) coincide for a certain value of  $y_1$  ( $0 < y_1 < 1$ ),  $0 < z_1 < 1$  fixed. We denote this value by  $y_1^{(k_1, k_2)} = y_1^{(k_1, k_2)}(z_1)$ , it still depends on  $z_1$ . We note that the partial fractioning can still be performed for arbitrary values of  $y_1$  and  $z_1$  as long as  $\epsilon$  and  $\epsilon'$  are kept finite. By carefully taking the limit  $\epsilon \rightarrow 0$  in the terms containing  $k_1^2$  and  $\epsilon' \rightarrow 0$  in the terms containing  $k_2^2$  and using Eq. (B3) one ends up with

$$I^{(k_1, k_2)}(y_1, z_1) = \frac{1}{x_1^{(k_1)} - x_1^{(k_2)} + i\tilde{\epsilon}} \left\{ \left( \frac{\partial k_2^2}{\partial x_1} \right)^{-1} \int_0^1 dx_1 \frac{h(x_1, y_1, z_1) - h(x_1^{(k_1)}, y_1, z_1)}{k_1^2} + \left( \frac{\partial k_2^2}{\partial x_1} \right)^{-1} h(x_1^{(k_1)}, y_1, z_1) \left( \oint \int_0^1 \frac{dx_1}{k_1^2} - i\pi \left| \frac{\partial k_1^2}{\partial x_1} \right|^{-1} \right) - \left( \frac{\partial k_1^2}{\partial x_1} \right)^{-1} \int_0^1 dx_1 \frac{h(x_1, y_1, z_1) - h(x_1^{(k_2)}, y_1, z_1)}{k_2^2} - \left( \frac{\partial k_1^2}{\partial x_1} \right)^{-1} h(x_1^{(k_2)}, y_1, z_1) \left( \oint \int_0^1 \frac{dx_1}{k_2^2} - i\pi \left| \frac{\partial k_2^2}{\partial x_1} \right|^{-1} \right) \right\} . \quad (\text{B6})$$

In Eq. (B6)  $\tilde{\epsilon}$  stands for either  $\epsilon$  or  $\epsilon'$ . Closer inspection of  $(x_1^{(k_1)} - x_1^{(k_2)})$  (considered as function of  $y_1$ ) reveals that the zero  $y_1^{(k_1, k_2)}$  is quadratic. On the other hand, one also finds that  $y_1^{(k_1, k_2)}$  is a single zero of both  $h(x_1^{(k_1)}, y_1, z_1)$  and  $h(x_1^{(k_2)}, y_1, z_1)$ . This immediately implies that the real part of  $I^{(k_1, k_2)}(y_1, z_1)$  is a regular function of  $y_1$  and also  $z_1$  so that Gaussian quadrature is again applicable to the corresponding integrations. Taking further into account that  $(\partial k_1^2 / \partial x_1)^{-1}$  and  $(\partial k_2^2 / \partial x_1)^{-1}$  have different signs the imaginary part of  $I^{(k_1, k_2)}(y_1, z_1)$  can be written as

$$\text{Im} I^{(k_1, k_2)}(y_1, z_1) = 2\pi \left( \frac{\partial^2 (x_1^{(k_1)} - x_1^{(k_2)})}{\partial y_1^2} \right)^{-1} \left( \frac{\partial k_1^2}{\partial x_1} \right)^{-1} \left| \frac{\partial k_2^2}{\partial x_1} \right|^{-1} [\tilde{h}(x_1^{(k_1)}, y_1, z_1) + \tilde{h}(x_1^{(k_2)}, y_1, z_1)] \frac{(y_1 - y_1^{(k_1, k_2)})}{(y_1 - y_1^{(k_1, k_2)})^2 + i\tilde{\epsilon}} , \quad (\text{B7})$$

where  $h = (y_1 - y_1^{(k_1, k_2)})\tilde{h}$ . Integrating  $\text{Im} I^{(k_1, k_2)}$  with respect to  $y_1$  and letting  $\tilde{\epsilon} \rightarrow 0$  gives

$$\int_0^1 dy_1 \text{Im} I^{(k_1, k_2)}(y_1, z_1) = \oint \int_0^1 dy_1 \text{Im} I^{(k_1, k_2)}(y_1, z_1) , \quad (\text{B8})$$

i.e., only the principle-value part of the integration survives. The principle-value integral in Eq. (B8) can be treated analogously to the principle-value integrals in  $x_1$  [cf. Eq. (B3)].

Proceeding along the steps outlined in this appendix, i.e.,

carefully separating the singular contributions, exploiting  $\delta$  functions, rewriting principal-value integrals as ordinary integrals plus analytically solvable principle-value integrals, it is finally possible to do all the numerical integrations by means of fixed-point Gaussian quadrature. For our purposes an  $x$ - $y$ - $z$  grid of  $20 \times 20 \times 24$  turned out to be sufficient. Taking instead a  $32 \times 32 \times 48$  grid changes the results by less than 0.2%. The numerical calculations were performed on a DEC7000-610 APLPHA workstation. For the larger grid size the calculation of  $d\sigma/dt(\gamma p \rightarrow K^+ \Lambda)$  took about 1 s per energy point and angle.

- [1] C. Bennhold, Phys. Rev. C **39**, 1944 (1989).
- [2] R. A. Adelseck and B. Saghai, Phys. Rev. C **42**, 108 (1990); **45**, 2030 (1992).
- [3] R. A. Williams, C. R. Ji, and S. R. Cotanch, Phys. Rev. C **46**, 1617 (1992).
- [4] T. Mart, C. Bennhold, and C. E. Hyde-Wright, Phys. Rev. C **51**, R1074 (1995).
- [5] R. A. Schumacher, Nucl. Phys. **A585**, 63c (1995).
- [6] E. Paul *et al.*, Prog. Part. Nucl. Phys. **34**, 201 (1995).
- [7] Z. Li, Phys. Rev. C **52**, 1648 (1995).
- [8] A. Donnachie, in *High Energy Physics V*, edited by E. H. S. Burhop (Academic, New York, London, 1972).
- [9] J. F. Gunion, S. J. Brodsky, and R. Blankenbecler, Phys. Rev. D **8**, 287 (1973).
- [10] For a review of hard exclusive processes and further references see, e.g., S. J. Brodsky and G. P. Lepage, in *Perturbative Quantum Chromodynamics*, edited by A. H. Mueller (World Scientific, Singapore, 1989).
- [11] V. L. Chernyak and A. R. Zhitnitsky, Phys. Rep. **112**, 173 (1984).
- [12] G. R. Farrar, H. Zhang, A. A. Ogloblin, and I. R. Zhitnitsky, Nucl. Phys. **B311**, 585 (1988).
- [13] V. L. Chernyak, A. A. Ogloblin, and I. R. Zhitnitsky, Z. Phys. C **42**, 569 (1989).
- [14] N. G. Stefanis, Acta Phys. Pol. B **25**, 1777 (1994).
- [15] P. Kroll, in *Photon 95*, Proceedings of the Photon 95 Workshop, Sheffield, England, 1995, edited by U. J. Miller *et al.* (World Scientific, Singapore, 1995); R. Jakob, P. Kroll, and M. Raulfs, J. Phys. G **22**, 45 (1996); P. Kroll and M. Raulfs, Phys. Lett. B **387**, 848 (1996).
- [16] J. Bolz and P. Kroll, Z. Phys. A **356**, 327 (1996).
- [17] V. Braun and I. Halperin, Phys. Lett. B **328**, 457 (1994).
- [18] A. Radyushkin, Nucl. Phys. **B325**, 141c (1991).
- [19] G. R. Farrar, K. Huleihel, and H. Zhang, Nucl. Phys. **B349**, 655 (1991).
- [20] R. Jakob, P. Kroll, M. Schürsmann, and W. Schweiger, Z. Phys. A **347**, 109 (1993).
- [21] P. Kroll, Th. Pilsner, M. Schürsmann, and W. Schweiger, Phys. Lett. B **316**, 546 (1993).
- [22] P. Kroll, M. Schürsmann, and P. A. M. Guichon, Nucl. Phys. **A598**, 435 (1996).
- [23] R. Jakob, Phys. Rev. D **50**, 5647 (1994).
- [24] M. Anselmino, P. Kroll, and B. Pire, Z. Phys. C **36**, 89 (1987); P. Kroll, in *Spin and Polarization Dynamics in Nuclear and Particle Physics*, Trieste, Italy, 1988, edited by A. O. Barut, Y. Onel, and A. Penzo (World Scientific, Singapore, 1990).
- [25] E. V. Shuryak, Phys. Rep. **115**, 151 (1984).
- [26] M. Virchaux and A. Milsztajn, Phys. Lett. B **274**, 221 (1992).
- [27] M. Szczekowski, in *Quark Cluster Dynamics*, Proceedings of the International Workshop on Quark Cluster Dynamics, Bad Honnef, Germany, 1992, edited by K. Goeke, P. Kroll, and H. Petry, Lecture Notes in Physics Vol. 417 (Springer, Berlin, 1993).
- [28] M. Benayoun and V. L. Chernyak, Nucl. Phys. **B329**, 285 (1990).
- [29] B. Chibisov and A. R. Zhitnitsky, Phys. Rev. D **52**, 5273 (1995).
- [30] T. Huang, in *Hadronic Matrix Elements and Weak Decays*, Proceedings of the Workshop, Ringberg Castle, Germany, edited by A. J. Buras *et al.* [Nucl. Phys. B (Proc. Suppl.) **7**, 320 (1989)].
- [31] J. D. Bjorken and S. D. Drell, *Relativistic Quantum Fields* (McGraw-Hill, New York, 1965).
- [32] I. S. Barker, A. Donnachie, and J. K. Storrow, Nucl. Phys. **B95**, 347 (1975).
- [33] F. Tabakin, Nucl. Phys. **A570**, 311c (1994).
- [34] J. Küblbeck, M. Böhm, and A. Denner, Comput. Phys. Commun. **60**, 165 (1990).
- [35] R. Mertig, M. Böhm, and A. Denner, Comput. Phys. Commun. **64**, 345 (1991).
- [36] R. Kleiss and W. J. Stirling, Nucl. Phys. **B262**, 235 (1985).
- [37] M. Schürsmann, Ph.D. thesis, Wuppertal University, 1992.
- [38] J. A. M. Vermaseren, *Symbolic Manipulation in FORM* (Computer Algebra Nederland, Amsterdam, 1991).
- [39] R. L. Anderson *et al.*, Phys. Rev. D **14**, 679 (1976).
- [40] S. Ong, Phys. Rev. D **52**, 3111 (1995).
- [41] A. S. Kronfeld and B. Nižič, Phys. Rev. D **44**, 3445 (1991).
- [42] G. R. Farrar, G. Sterman, and H. Zhang, Phys. Rev. Lett. **62**, 2229 (1989).
- [43] G. Vogel *et al.*, Phys. Lett. **40B**, 513 (1972).
- [44] W. A. Crabb *et al.*, Phys. Rev. Lett. **65**, 3241 (1990).
- [45] G. Bunce *et al.*, Phys. Rev. Lett. **36**, 1113 (1976).
- [46] S. J. Brodsky and G. R. Farrar, Phys. Rev. Lett. **31**, 1153 (1973).
- [47] J. Bolz, R. Jakob, P. Kroll, M. Bergmann, and N. G. Stefanis, Z. Phys. C **66**, 267 (1995).
- [48] R. Jakob, Ph.D. thesis, Wuppertal University, 1993.
- [49] R. Jakob and P. Kroll, Phys. Lett. B **315**, 463 (1993); **319**, 545(E) (1993).
- [50] G. Folberth, R. Rossmann, and W. Schweiger, Saclay Report No. DAPNIA-SPhN-96-35 (unpublished).
- [51] S. D. Drell and T. M. Yan, Phys. Rev. Lett. **24**, 181 (1970).
- [52] G. P. Lepage and S. J. Brodsky, Phys. Rev. D **22**, 2157 (1980).
- [53] J. Arvieux and B. Pire, Prog. Part. Nucl. Phys. **35**, 299 (1995).